BIOCHEMISTRY
including biophysical chemistry & molecular biology

Article

pubs.acs.org/biochemistry

Structures of *Mycobacterium tuberculosis* Anthranilate Phosphoribosyltransferase Variants Reveal the Conformational Changes That Facilitate Delivery of the Substrate to the Active Site

Tammie V. M. Cookson,[†] Genevieve L. Evans,[‡,§] Alina Castell,[‡,∥] Edward N. Baker,[‡] J. Shaun Lott,[‡] and Emily J. Parker*[,†]

[†]Maurice Wilkins Centre for Molecular Biodiscovery, Biomolecular Interaction Centre, and Department of Chemistry, University of Canterbury, 20 Kirkwood Avenue, Christchurch 8140, New Zealand

[‡]Maurice Wilkins Centre for Molecular Biodiscovery and School of Biological Sciences, University of Auckland, 3 Symonds Street, Auckland 1142, New Zealand

Supporting Information

ABSTRACT: Anthranilate phosphoribosyltransferase (AnPRT) is essential for the biosynthesis of tryptophan in *Mycobacterium tuberculosis* (*Mtb*). This enzyme catalyzes the second committed step in tryptophan biosynthesis, the Mg^{2+}-dependent reaction between 5′-phosphoribosyl-1′-pyrophosphate (PRPP) and anthranilate. The roles of residues predicted to be involved in anthranilate binding have been tested by the analysis of six *Mtb*-AnPRT variant proteins. Kinetic analysis showed that five of six variants were active and identified the conserved residue R193 as being crucial for both anthranilate binding and catalytic function. Crystal structures of these *Mtb*-AnPRT variants reveal the ability of anthranilate to bind in three sites along an extended anthranilate tunnel and expose the role of the mobile $\beta2-\alpha6$ loop in facilitating the enzyme's sequential reaction mechanism. The $\beta2-\alpha6$ loop moves sequentially between a "folded" conformation, partially occluding the anthranilate tunnel, via an "open" position to a "closed" conformation, which supports PRPP binding and allows anthranilate access via the tunnel to the active site. The return of the $\beta2-\alpha6$ loop to the "folded" conformation completes the catalytic cycle, concordantly allowing the active site to eject the product PRA and rebind anthranilate at the opening of the anthranilate tunnel for subsequent reactions. Multiple anthranilate molecules blocking the anthranilate tunnel prevent the $\beta2-\alpha6$ loop from undergoing the conformational changes required for catalysis, thus accounting for the unusual substrate inhibition of this enzyme.

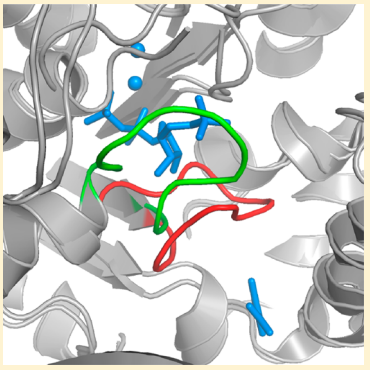

Tuberculosis (TB) is a global epidemic,[1,2] with many drug-resistant strains of the causative agent, *Mycobacterium tuberculosis* (*Mtb*), emerging that counteract previously effective chemotherapeutic efforts to eradicate infection.[3,4] With treatment options becoming more limited, further understanding of *Mtb* cell biology is necessary to develop novel anti-TB drugs.

The biosynthesis of the aromatic amino acid tryptophan from chorismate has been demonstrated to be necessary for the survival of *Mtb* within the host.[5] One host immune response upon infection with *Mtb* is the activation of a tryptophan starvation response initiated by CD4 T-cells.[5] The presence of the tryptophan biosynthetic pathway within *Mtb* counteracts this host immune response, allowing the bacterium to survive within the macrophage. Auxotrophic mutants of *Mtb* that contain gene knockouts in the tryptophan pathway are unable to replicate in cultured murine macrophages and also show an attenuation of virulence in immune-competent mice.[6] A knockout strain of *Mtb* that has the gene (*trpD*; Rv2192c) encoding anthranilate phosphoribosyltransferase (AnPRT, EC 2.4.2.18) removed is unable to cause disease, even in mice deficient in CD4 T-cells.[6] These results highlight the potential of this enzyme as a drug target.

AnPRT is a member of the phosphoribosyltransferase (PRT) enzyme family. These enzymes catalyze the transfer of the phosphoribosyl group of 5′-phosphoribosyl-1′-pyrophosphate (PRPP) to a nitrogenous and usually aromatic base.[7,8] The glycosidic bond between the C1 atom of the ribose ring and the oxygen of the pyrophosphate (PP_i) moiety of PRPP is cleaved in this process. The reaction proceeds with inversion of stereochemistry at the anomeric carbon and requires Mg^{2+} for catalysis.[9] Four subfamilies of PRTs have been identified,[8,9] with AnPRT defined as a type III PRT. AnPRT catalyzes the second committed step of the tryptophan biosynthetic pathway, converting PRPP and anthranilate to *N*-(5′-phosphoribosyl)-anthranilate (PRA) and PP_i (Figure 1). Type I PRTs make up a homologous group of enzymes that are part of the nucleotide synthesis and salvage pathways.[9] Examples of type II PRTs can

Received: June 4, 2015
Revised: August 24, 2015
Published: September 10, 2015

ACS Publications © 2015 American Chemical Society

DOI: 10.1021/acs.biochem.5b00612
Biochemistry 2015, 54, 6082−6092

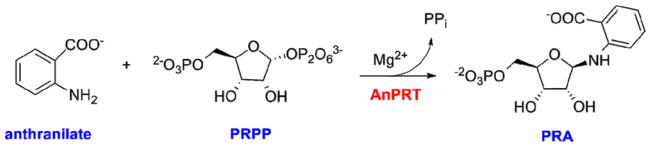

Figure 1. Reaction catalyzed by AnPRT.

be found in quinolinic acid PRT (NAD biosynthesis)[10] and nicotinic acid PRT (NAD salvage).[11] Type IV PRTs are solely represented by ATP-PRT, which catalyzes the first step of the histidine biosynthetic pathway.[12]

AnPRT is homodimeric,[13,14] with each chain consisting of a smaller N-terminal domain consisting of six α-helices and a larger C-terminal domain in which eight α-helices surround a central seven-stranded β-sheet. One active site is present per chain (Figure 2), located in the hinge region between the N-

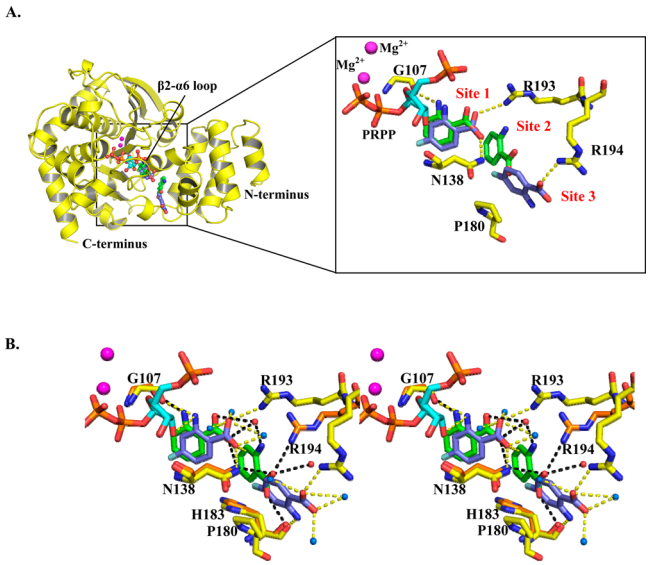

Figure 2. *Mtb*-AnPRT (Protein Data Bank entry 4N5V)[19] and *Sso*-AnPRT (Protein Data Bank entry 1ZYK)[17] anthranilate binding sites. (A) *Mtb*-AnPRT chain with a close-up of the active site. *Mtb*-AnPRT (yellow) with PRPP (cyan), 4-fluoroanthranilate (4FA, purple), and Mg^{2+} (magenta spheres) bound is overlaid with *Sso*-AnPRT (not shown) with PRPP (not shown), Mg^{2+} (not shown), and anthranilate (green) bound. Anthranilate binding sites are denoted with red text. Polar contacts between *Mtb*-AnPRT and the 4FA molecules are indicated by yellow dashes. (B) Stereodiagram of *Sso*-AnPRT (orange) with PRPP (not shown), Mg^{2+} (not shown), and anthranilate (green) bound overlaid with *Mtb*-AnPRT (yellow) with PRPP (cyan), Mg^{2+} (magenta spheres), and 4FA (purple) bound. Polar contacts for anthranilate are shown as black dashes, with polar contacts for 4FA shown as yellow dashes. Water molecules from *Sso*-AnPRT are shown as red spheres and *Mtb*-AnPRT water molecules as blue spheres.

and C-terminal domains, as is observed for the orthologous AnPRT enzymes from *Sulfolobus solfataricus*, *Pectobacterium carotovorum*, *Thermus thermophilus*, *Xanthomonas campestris*, *Anabaena* sp. PCC7120, and *Acinetobacter baylyi*.[13,15,16] The substrate PRPP binds to *Mtb*-AnPRT at the bottom of a deep cleft in the C-terminal domain and is surrounded by two flexible loops (β1−α5 and β2−α6) that rearrange around PRPP upon binding.[14] Initially, two anthranilate binding sites were predicted within *Mtb*-AnPRT by Lee et al.[14] using *in silico* docking, despite the 1:1 reaction stoichiometry with PRPP: an inner, catalytically relevant site directly adjacent to the PRPP binding site (site 1) and a second site more distal to PRPP [site 2 (Figure 2)]. These two anthranilate binding sites were located within an "anthranilate tunnel" and are analogous to those observed in crystal structures of *S. solfataricus* AnPRT.[17]

Anthranilate-like inhibitors and alternative substrates, such as 4-fluoroanthranilate (4FA), have since been observed bound to wild-type *Mtb*-AnPRT, both in site 1 and in an additional outer site not predicted by *in silico* docking, located at the entrance to the anthranilate tunnel [site 3 (Figure 2)].[18−20] The protein contacts required for anthranilate binding in site 1 are not properly arranged unless PRPP is bound,[14] consistent with the sequential mechanism observed for *Mtb*-AnPRT.[19] The binding of alternative anthranilate-like substrates in site 3, however, has been observed to precede PRPP binding, with binding at the outer site 3 suggested as a means of effectively sequestering anthranilate for immediate reaction upon PRPP binding.[19] It has also been suggested that the binding of anthranilate in site 3 is responsible for the observed substrate inhibition of *Mtb*-AnPRT.[19] After binding in site 3, it is proposed that anthranilate molecules migrate toward site 1, the catalytically relevant binding site. At higher concentrations of anthranilate, a second anthranilate molecule could bind in site 3 during the migration of the first anthranilate molecule from site 3 to site 1, and this may account for the substrate inhibition observed for this enzyme.

This study explores the roles of the residues lining the anthranilate binding tunnel. Variants of *Mtb*-AnPRT in which residues G107, N138, P180, R193, and R194 are mutated are shown to have impaired catalytic function. The reduced catalytic capabilities of these variant proteins have allowed the capture of crystal structures at various stages of catalysis, helping to unravel the sequence of catalytic events utilized by *Mtb*-AnPRT, and the role of the anthranilate tunnel and the flexible β2−α6 loop for delivering catalytic function.

EXPERIMENTAL PROCEDURES

Cloning, Expression, and Purification. Wild-type *Mtb*-AnPRT was expressed and purified as previously described.[14,18,19] Mutants of the wild-type *trpD* plasmid were made by site-directed mutagenesis, using the primers listed in Table S1 of the Supporting Information and the wild-type *trpD* plasmid as a template. The vectors bearing the genes for the *Mtb*-AnPRT variants were then transformed into *Escherichia coli* BL21(DE3) pBB528/pBB541 cells for expression and purification.[21]

The variant *Mtb*-AnPRTs were expressed as described for wild-type AnPRT[14,18] and purified using immobilized metal affinity chromatography (IMAC). IMAC employed a pre-charged Ni^{2+}-Sepharose High Performance resin packed in a HisTrap HP column (GE Healthcare) at 4 °C. The supernatant liquid was passed onto the column in lysis buffer [50 mM Tris-HCl (pH 8.0), 200 mM NaCl, and 25 mM imidazole], with proteins that eluted from the column using a gradient of increasing imidazole concentration (linear) from 25 to 200 mM over 50 mL at a flow rate of 2−3 mL min^{-1}. Fractions containing variant *Mtb*-AnPRTs (as determined by gel electrophoresis) were pooled and passed through a HiPrep 26/10 desalting column prepacked with Sephadex G-25 Fine (GE Healthcare) at 4 °C, in either lysis buffer or crystallization buffer (50 mM Tris-HCl, 150 mM NaCl, and 5% glycerol) depending on the future use of the protein. The elution flow rate was 2−5 mL min^{-1}. Variant proteins were then

DOI: 10.1021/acs.biochem.5b00612
Biochemistry 2015, 54, 6082−6092

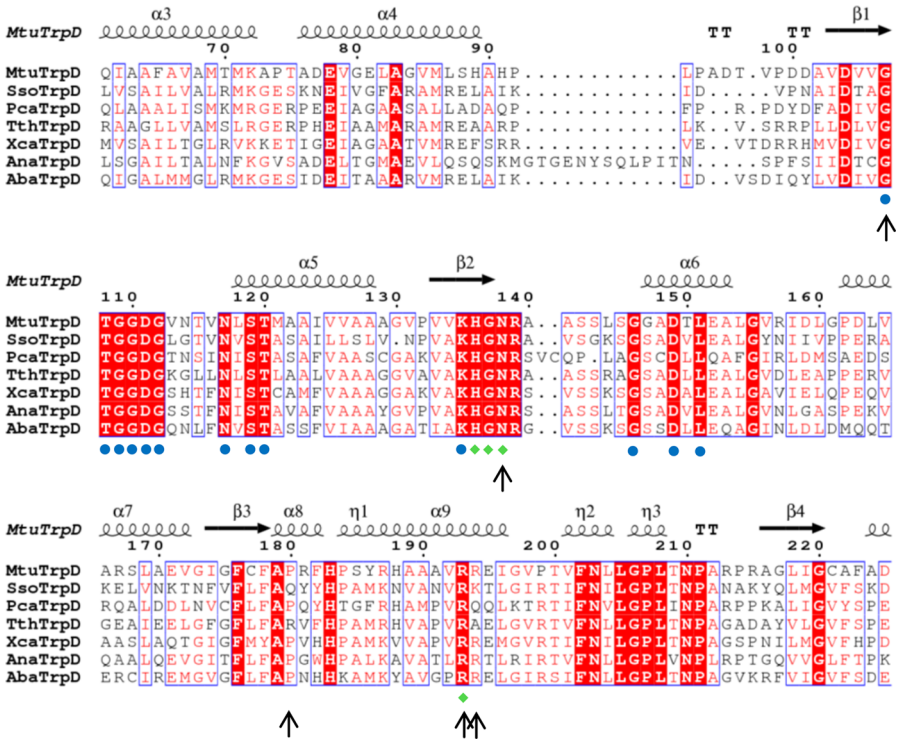

Figure 3. Structure-based sequence alignment of AnPRT enzymes from *M. tuberculosis* (*Mtb*; PDB entry 3QR9), *S. solfataricus* (*Sso*; PDB entry 1ZYK), *P. carotovorum* (*Pca*; PDB entry 1KGZ), *T. thermophilus* (*Tth*; PDB entry 1V8G), *X. campestris* (*Xca*; PDB entry 4HKM), *Anabaena* sp. PCC7120 (*Ana*; PDB entry 1VQU), and *A. baylyi* (*Aba*; PDB entry 4GTN) using TCOFFEE:Expresso.[33] AnPRT sequences were selected for this alignment on the basis of the availability of their crystal structures in the PDB. The diagram was made using ESPript 3.0.[34] The *Mtb*-AnPRT secondary structure elements are indicated above the alignment, where TT indicates a strict β-turn. Markers indicate residues postulated to be involved in PRPP binding (blue circles) and anthranilate binding (green diamonds). Arrows indicate residues investigated in this study. Coloring of the residues is indicative of residue conservation, with darker red areas indicating a higher degree of conservation.

concentrated as previously described,[14,18] flash-frozen with liquid N_2, and stored at −80 °C.

Biochemical Assays. The kinetic parameters of both wild-type and variant *Mtb*-AnPRTs were determined using an enzyme-coupled UV/vis-based assay in which the formation of indole glycerol phosphate (InGP) is detected at 270 nm as previously described.[18] *E. coli* PRA isomerase-InGP synthase protein was expressed and purified as previously described for use in the coupled assay.[18] The following components were used in the assay: *Mtb*-AnPRT variant (0.1−1 μM), $MgCl_2$ (1 mM), *Eco*-PRAI:InGPS (3−10 μM, held at a minimum 10-fold excess), PRPP (either held at 0.6 mM for determination of anthranilate parameters or varied from 0 to 560 μM), anthranilate (either held at the concentration at which maximal activity was observed for determination of PRPP parameters or varied from 0 to 1 mM), and Tris-HCl buffer [50 mM Tris-HCl and 150 mM NaCl (pH 8.0)]. The concentration of the inactive variant *Mtb*-G107P was increased from 0.5 to 1.2 μM during experiments and was tested in the presence of ≤1 mM PRPP and ≤1 mM anthranilate.

Solutions were equilibrated at 25 °C and reactions initiated by the addition of variant *Mtb*-AnPRT, with initial rates of reaction determined by a least-squares fit of the initial rate data. Raw data were fitted to either the Michaelis−Menten equation

$$v = \frac{v_{max}[S]}{K_M + [S]}$$

or the substrate inhibition equation

$$v = \frac{v_{max}[S]}{K_M + [S]\left(1 + \frac{[S]}{K_i}\right)}$$

using GraFit 5 (Erithacus Software).

Crystallization. Crystals of variant *Mtb*-AnPRTs were grown by hanging-drop vapor diffusion in 24-well VDX plates (Hampton Research). Protein solutions (3−7 mg mL^{-1}), in 50 mM Tris-HCl (pH 8.0), 150 mM NaCl, and 5% glycerol (v/v), were mixed 1:1 (v/v) with a reservoir solution containing 200 mM sodium imidazole malate (pH 6.5−8.0) and 5−15% PEG-4000. The additives (PRPP, $MgCl_2$, and anthranilate) were each present at a concentration of 10 mM. All additives were cocrystallized with *Mtb*-AnPRT with the exception of anthranilate, which was soaked into the crystal in the presence of 26% glycerol and the crystallization mother liquor. Droplets (2 μL) were seeded with wild-type *Mtb*-AnPRT crystals using a cat whisker. Crystals typically began to form after 4 h and were fully formed in 24 h, displaying a diamond-like morphology. Crystallization trays were left at 20 °C until immediately before data collection, with crystals removed from the crystallization drop with a nylon loop. Crystals were immersed briefly in a cryoprotectant solution (26% glycerol in the respective reservoir solution) before being stored in liquid N_2.

Data Collection and Refinement. X-ray diffraction data were collected at the Australian Synchrotron using the MX1 and MX2 beamlines and were indexed, integrated, and scaled using XDS[22] and either SCALA or AIMLESS.[23,24] The structures of the variant *Mtb*-AnPRTs were determined by molecular replacement (Phaser MR-CCP4),[25] using the

DOI: 10.1021/acs.biochem.5b00612
Biochemistry 2015, 54, 6082−6092

Table 1. Kinetic Data[a] for Wild-Type and Variant *Mtb*-AnPRTs

Mtb-AnPRT variant	K_M Anth (μM)	K_M PRPP (μM)	k_{cat} (s^{-1})	k_{cat}/K_M Anth (μM^{-1} s^{-1})	k_{cat}/K_M PRPP (μM^{-1} s^{-1})	K_i Anth (μM)
wild-type	2.0 ± 0.2	48 ± 2	1.9 ± 0.06	0.95 ± 0.13	0.040 ± 0.003	47 ± 7
N138A	8.0 ± 0.6	160 ± 20	1.0 ± 0.02	0.13 ± 0.01	0.006 ± 0.001	*b*
R193A	480 ± 24	40 ± 4	0.075 ± 0.002	0.00016 ± 0.00002	0.0019 ± 0.0003	*d*
R193L	300 ± 18	48 ± 5	0.035 ± 0.001	0.000117 ± 0.000009	0.0007 ± 0.0001	*d*
P180A	4.0 ± 0.3	68 ± 5	1.7 ± 0.05	0.43 ± 0.04	0.025 ± 0.003	440 ± 110
R194A	5.8 ± 0.4	46 ± 3	1.9 ± 0.05	0.33 ± 0.03	0.041 ± 0.004	89 ± 11
G107P	*c*	*c*	*c*	*c*	*c*	*c*

[a]Reported errors are indicative of the standard deviation across triplicate measurements. [b]Substrate inhibition was not observed up to 220 μM anthranilate. [c]Activity could not be detected above 0.001 s^{-1}. [d]Variants that were not tested for substrate inhibition as their low activity demands the use of anthranilate concentrations that exceed the upper detection limit of the equipment.

structure of ligand-free wild-type *Mtb*-AnPRT [Protein Data Bank (PDB) entry 3QR9] as a template. Refinement and model building were performed using Refmac5[26] and WinCOOT,[27] respectively. The validation tools of COOT and MolProbity[28] were used to check for, and correct, conformational errors in the model. After the model and electron density were judged to be in good agreement in all regions apart from the ligand binding site(s) of interest, the electron density in the ligand binding site(s) was examined. If appropriate electron density was present, the ligand(s) of interest and water molecules were added to the model and the final rounds of refinement conducted. Ligand restraints were generated by using the PRODRG server.[29] The occupancies of ligands of interest were refined by inspection of the electron density maps after refinement. The final refinement statistics for all the variant structures are listed in Table S2 of the Supporting Information. Atomic coordinates and structure amplitudes have been deposited with the PDB, with the accession codes listed in Table S2 of the Supporting Information. Figures illustrating structural details show chain A, unless otherwise stated, and were prepared by use of PyMOL[30] with maps generated using the FFT program[31] in the CCP4 suite.[24] The superimposed structures were also generated using PyMOL.

RESULTS

Selection of Variants. A structure-based alignment of sequences of the currently available structures of AnPRT is shown in Figure 3. *Mtb*-AnPRT residue N138 is located within a conserved $\psi\psi$KHGN motif spanning residues 133−138 (where ψ is a hydrophobic amino acid) on the flexible $\beta2-\alpha6$ loop. In previously described structures of *Mtb*-AnPRT, N138 interacts with both PRPP and anthranilate, forming hydrogen bonds with the C3 hydroxyl of PRPP via its backbone carbonyl oxygen, and with anthranilate (site 1) via its side chain amide nitrogen (Figure 2).[14,18−20] The variant protein *Mtb*-N138A was thus generated to test the role of this residue in delivering AnPRT function. Previous crystal structures have shown that a conserved arginine residue R193, located on helix $\alpha8$, forms a hydrogen bond to the anthranilate carboxylate group (site 1) via its guanidinium side chain[14,18−20] (Figure 2). The equivalent residue in *Sso*-AnPRT (R164) has been shown to be crucial for anthranilate binding and enzymatic catalysis.[17] Two variants were therefore made to investigate the role of the R193 side chain in *Mtb*-AnPRT: *Mtb*-R193A and *Mtb*-R193L.

An absolutely conserved GTGGD motif from residue 107 to 111 of *Mtb*-AnPRT is located on the $\beta1-\alpha5$ loop and is involved in PRPP binding. Previous structures show that G107 interacts with the PP_i group of PRPP via its peptide NH group, and also with the amino group of anthranilate in site 1 via its main chain carbonyl oxygen,[14,18−20] suggesting a role for this residue in supporting catalysis (Figure 2). Variant *Mtb*-G107P was synthesized to investigate the effects of removing the residue 107 NH group and reducing the flexibility of the $\beta1-\alpha5$ loop by introducing a conformationally restricted proline residue.

Crystal structures of *Mtb*-AnPRT with various anthranilate-like ligands bound have also identified the possible involvement of the nonconserved residues P180 and R194 in anthranilate binding at site 3.[18,19] The guanidinium group in the side chain of R194 forms a hydrogen bond to the carboxylate group of anthranilate, and the pyrrolidine ring of P180 interacts with the aromatic π orbitals of anthranilate via CH···π contacts (Figure 2).[18,32] The two variants *Mtb*-R194A and *Mtb*-P180A were thus generated to investigate the effect of removing each side chain to probe the role of the outer site (site 3) in the catalytic function of *Mtb*-AnPRT.

Physical and Kinetic Characterization of *Mtb*-AnPRT Variants. All *Mtb*-AnPRT variants were successfully expressed and purified and physically characterized using mass spectrometry and circular dichroism, with results indicating that all variants were of the expected mass and folded correctly (Figure S1 and Table S3 of the Supporting Information).

Kinetic parameters were determined for all variants of *Mtb*-AnPRT with the exception of *Mtb*-G107P, which was determined to be catalytically inactive under experimental conditions (Table 1 and Figure S2 of the Supporting Information). Two variants, *Mtb*-P180A and *Mtb*-R194A, showed k_{cat} values similar to that of the wild-type enzyme. These two enzyme variants displayed apparent PRPP K_M values similar to that of the wild-type enzyme and slightly elevated apparent K_M values for anthranilate. The k_{cat} value of the N138A variant was reduced 2-fold in comparison to that of the wild-type enzyme. This enzyme also displayed a 4-fold increase in anthranilate K_M and a 3-fold increase in PRPP K_M versus the wild-type enzyme values.

Apart from inactive *Mtb*-G107P, the most striking impairments to catalytic activity were observed for variants *Mtb*-R193A and *Mtb*-R193L. The turnover numbers of *Mtb*-R193A and *Mtb*-R193L were decreased by factors of 25 and 54, respectively, compared with that of the wild-type enzyme. Both variants displayed anthranilate K_M values considerably higher than that of the wild-type enzyme, with 240- and 150-fold increases observed, respectively, indicating a critical role for R193 in both anthranilate binding and efficient catalytic turnover of PRPP and anthranilate. Similar results were observed for alanine substitution of the equivalent residue in *Sso*-AnPRT (*Sso*-R164A), which demonstrated a 7000-fold increase in the apparent K_M for anthranilate and a 7-fold

DOI: 10.1021/acs.biochem.5b00612
Biochemistry 2015, 54, 6082−6092

Table 2. Observations from Crystal Structures of Variant *Mtb*-AnPRTs

structure label	variant	ligands present in crystal mother liquor	ligands observed bound in the *Mtb*-AnPRT structure		β2−α6 loop conformation	
			chain A	chain B	chain A	chain B
A	*Mtb*-N138A	PRPP, Mg^{2+}	PRPP, Mg^{2+}	none	closed	folded[a]
B	*Mtb*-P180A	PRPP, Mg^{2+}	PRPP (alternative conformation)	PRPP, Mg^{2+} (alternative conformation[b])	open	closed
C1	*Mtb*-R193A	PRPP, Mg^{2+}	none	none	folded	folded
C2		PRPP, Mg^{2+}, Anth (3 s soak)	Anth	Anth	folded[a]	folded
D1	*Mtb*-R193L	PRPP, Mg^{2+}	PRPP, Mg^{2+}	PRPP, Mg^{2+}	closed	closed
D2		PRPP, Mg^{2+}, Anth (5 s soak)	PRPP, Mg^{2+}	PP_i, Mg^{2+}	closed	folded
E	*Mtb*-R194A	PRPP, Mg^{2+}, Anth (5 min soak)	PP_i, Mg^{2+}, Anth (sites 1 and 2)	PP_i, Mg^{2+}, Anth (sites 1 and 3)	disordered	disordered

[a]There is sufficient electron density to determine the overall conformation of the loop, although some sections of the loop are not well-defined. Alternative conformation indicates that the PRPP is in an alternate conformation from that observed in wild-type *Mtb*-AnPRT. [b]The alternate conformation is at an occupancy of 0.2. Protein concentrations ranged from 3 to 7 mg mL^{-1}. Data collection and refinement parameters are provided in Table S2 of the Supporting Information. Observations from other previously reported AnPRT structures are provided in Table S4 of the Supporting Information for comparison. Root-mean-square deviation values of the variant structures compared to *Mtb*-AnPRT wild-type structures are listed in Table S5 of the Supporting Information.

decrease in the turnover number compared with that of wild-type *Sso*-AnPRT.[17]

Anthranilate inhibition of wild-type *Mtb*-AnPRT has previously been reported.[19] To investigate whether the outer anthranilate binding site, site 3, plays a role in the observed anthranilate inhibition, *Mtb*-N138A, *Mtb*-P180A, and *Mtb*-R194A were tested with high concentrations of anthranilate (Table 2 and Figure S3 of the Supporting Information). *Mtb*-P180A and *Mtb*-R194A both demonstrated an intact capacity for anthranilate inhibition, although increases in the K_i values of 9- and 2-fold, respectively, were observed, indicating that the outer anthranilate binding site (site 3) does contribute to the substrate inhibition observed for this enzyme. Unexpectedly, *Mtb*-N138A, which has decreased apparent affinities for PRPP (3-fold increase in K_M) and for anthranilate (4-fold increase in K_M), showed no signs of anthranilate inhibition, indicating the conserved residue N138 plays a role in *Mtb*-AnPRT anthranilate inhibition.

Crystal Structures of *Mtb*-AnPRT Variants. Crystal structures were obtained for all of the *Mtb*-AnPRT variants (Table 2) with the exception of *Mtb*-G107P, which did not crystallize despite considerable efforts. The variants were cocrystallized with PRPP and Mg^{2+} to visualize their ability to bind these ligands. In addition, the variant cocrystals were soaked with anthranilate for various time periods prior to being flash-cooled, to capture PRPP and anthranilate within the active site simultaneously.

All protein variants crystallized as homodimers as has been observed in all previous structures reported for this enzyme.[14,18,19] All structures obtained in this study had two chains in the asymmetric unit. The crystal structures of variants *Mtb*-N138A, *Mtb*-P180A, and *Mtb*-R193L were successfully obtained with PRPP and Mg^{2+} present in the active site (Table 2, structures A, B, and D1, respectively), but these substrates were not observed bound in *Mtb*-R193A (Table 2, structure C1). Anthranilate soaks of crystals pre-exposed to PRPP and Mg^{2+} yielded structures of *Mtb*-R193A and *Mtb*-R194A with anthranilate bound in the anthranilate tunnel (Table 2, structures C2 and E, respectively). These soaks were also performed with *Mtb*-R193L; chain A of the resulting crystal structure had PRPP and Mg^{2+} bound, whereas chain B had PP_i and Mg^{2+} bound (Table 2, structure D2).

PRPP and Mg^{2+} Binding in Variant *Mtb*-AnPRTs. The structure of *Mtb*-N138A was obtained with PRPP and Mg^{2+} bound at the active site (Table 2, structure A), with both chains showing PRPP and Mg^{2+} bound in a mode similar to that observed for the wild-type *Mtb*-AnPRT structure (Table S4, PDB entry 1ZVW[14]). The crystal structure of *Mtb*-R193L (Table 2, structure D1) also shows PRPP and Mg^{2+} bound in this way. In both these structures, the β2−α6 loop is in a closed conformation over the PRPP.

In chain A of *Mtb*-P180A (Table 2, structure B), an alternative PRPP binding mode was observed (Figure 4A). In this alternative conformation, the ribose ring of PRPP is rotated approximately 180° relative to its position in the wild-type protein structure, the C1-phosphate moiety is oriented toward the anthranilate binding tunnel, and the β2−α6 loop adopts an open conformation similar to that in the ligand-free wild-type structure. The PP_i moiety of the PRPP in this alternative binding mode forms hydrogen bonds with the invariant residues G107, S119, and K135 and the semiconserved residue T115 and overlaps with Mg^{2+} binding site Mg1 (Figure 4B). The ribose ring forms a hydrogen bond with the nonconserved N114 via its C3 hydroxyl and the semiconserved residue S145 via its C2 hydroxyl, with the phosphate moiety forming a hydrogen bond to a water molecule only.

The electron density for chain B of this *Mtb*-P180A structure (Table 2, structure B) shows that two PRPP binding modes can be adopted by this variant: one identical to that in the wild-type structure (PDB entry 1ZVW) at an occupancy of 0.8 and one in the alternative PRPP binding mode at an occupancy of 0.2 (Figure 4C). This alternative PRPP positioning has also been observed in a crystal structure of the *Sso*-AnPRT-D83G/F149S variant (Table S4, PDB entry 3GBR).[35] The binding of PRPP in its productive mode is associated with the closure of the β2−α6 loop.[14] The alternate binding mode for PRPP in *Mtb*-P180A is associated with the "open" conformation of the β2−α6 loop, suggesting that this structure may indicate the mode by which PRPP approaches the active site of *Mtb*-AnPRT prior to the closing of the β2−α6 loop. This interpretation is consistent with the presence of two PRPP binding modes, coupled with two β2−α6 loop conformations of the *Mtb*-P180A structure.

DOI: 10.1021/acs.biochem.5b00612
Biochemistry 2015, 54, 6082−6092

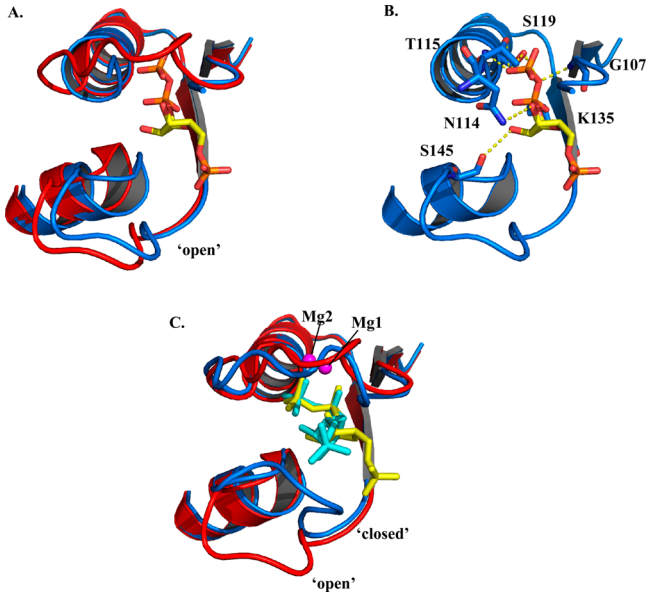

Figure 4. PRPP binding and $\beta2-\alpha6$ loop conformations in *Mtb*-P180A (structure B). (A) Structure B, chain A (blue) with PRPP bound overlaid on ligand-free wild-type *Mtb*-AnPRT (red, PDB entry 3QR9[18]). (B) Structure B, chain A (blue) with PRPP bound showing hydrogen bonds as yellow broken lines. (C) Structure B, chain B (blue) shown with PRPP and Mg^{2+} (magenta spheres) bound overlaid on ligand-free wild-type *Mtb*-AnPRT (red, PDB entry 3QR9), showing the closed and open $\beta2-\alpha6$ loop conformations, respectively. The cyan and yellow PRPP molecules in structure B correspond to conformations modeled with occupancy values of 0.8 and 0.2, respectively. Electron density maps are provided in Figure S4 of the Supporting Information.

Crystal Structures of *Mtb*-R193A Provide Insight into the Order of Ligand Binding for *Mtb*-AnPRT. Two crystal structures of the poorly active variant *Mtb*-R193A were obtained in this study: the first was obtained from protein crystallized in the presence of PRPP and Mg^{2+} (Table 2, structure C1), and the second was from a crystal further exposed to anthranilate soaking (Table 2, structure C2). Structure C1 was unexpectedly ligand-free, and comparisons with the wild-type *Mtb*-AnPRT ligand-free structure (Table S4, PDB entry 3QR9[18]) and the wild-type *Mtb*-AnPRT structure with PRPP and Mg^{2+} bound (PDB entry 1ZVW[14]) highlight an intriguing difference in the conformation of the $\beta2-\alpha6$ loop (Figure 5A). The wild-type ligand-free structure has the $\beta2-\alpha6$ loop in the "open" conformation, while the liganded structure shows the rearrangement of this loop around the PRPP substrate into the "closed" conformation. In structure C1, however, the $\beta2-\alpha6$ loop has a third conformation (labeled the "folded" conformation in Figure 5A), which partially occludes the anthranilate tunnel. The "folded" conformation is considerably different from both "closed" and "open" conformations, as indicated by the distances between the Cα atom positions of a central residue in the $\beta2-\alpha6$ loop, S142, in the "closed"/"open", "open"/"folded", and "closed"/"folded" forms of 6.0, 9.8, and 7.6 Å, respectively. The "folded" conformation has previously only been observed in wild-type *Mtb*-AnPRT with the alternative substrate 4FA bound in site 3 (Table S4, PDB entry 4N8Q).[19]

The second *Mtb*-R193A structure showed a single anthranilate molecule bound in site 3 in each chain (Table 2, structure C2). The $\beta2-\alpha6$ loops were again folded into the

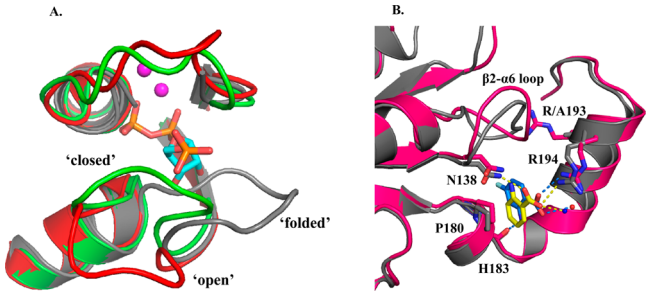

Figure 5. Alternative conformations of the $\beta2-\alpha6$ loop in *Mtb*-AnPRT. (A) Wild-type *Mtb*-AnPRT (green, PDB entry 1ZVW[14]) with PRPP (cyan) and Mg^{2+} (magenta spheres) bound overlaid on ligand-free wild-type *Mtb*-AnPRT (red, PDB entry 3QR9) and *Mtb*-R193A (structure C2) chain A (gray) with anthranilate (not shown) bound. An identical conformation of the $\beta2-\alpha6$ loop is observed in structure C2 chain B. (B) Structure C2 (gray) with anthranilate bound (yellow) overlaid on wild-type *Mtb*-AnPRT chain B (pink) with 4FA bound (blue, PDB entry 4N8Q[19]). Hydrogen bonds are depicted as yellow and blue dashes for anthranilate and 4FA, respectively. Water molecules are shown as blue or red spheres when bound to anthranilate or 4FA, respectively.

anthranilate tunnel (Figure 5B). This structure shows the anthranilate molecule forming hydrogen bonds to N138, R194, and a water molecule via its carboxylate group, with the aromatic ring oriented parallel to the P180 pyrrolidine ring. The positioning of anthranilate in site 3 is comparable to that of 4FA observed in the wild-type *Mtb*-AnPRT structure (PDB entry 4N8Q[19]) (Figure 5B). Previous studies of *Sso*-AnPRT have shown that anthranilate can bind to the enzyme in the absence of PRPP or Mg^{2+}.[17]

Pyrophosphate Is Observed in the *Mtb*-R193L Structure. Two crystal structures of the poorly active *Mtb*-R193L variant were also obtained. The crystal giving structure D1 was obtained in the presence of PRPP and Mg^{2+}, whereas the crystal giving structure D2 was additionally soaked with anthranilate prior to data collection. Both chains of structure D1 and chain A of structure D2 showed PRPP and Mg^{2+} bound in binding modes identical to that in wild-type *Mtb*-AnPRT (PDB entry 1ZVW). In contrast, chain B of structure D2 shows PP_i and Mg^{2+} bound in the active site, with the $\beta2-\alpha6$ loop in the "folded" conformation within the anthranilate tunnel. The PP_i is bound in the exact position found for the PP_i moiety in the wild-type *Mtb*-AnPRT structure with PRPP and Mg^{2+} bound (PDB entry 1ZVW), making contacts with invariant residues G107, S119, T120, K135, and G146 (Figure 6A). The formation of hydrogen bonds to the invariant residue N117, observed in the wild-type *Mtb*-AnPRT structure, is not observed in this structure as the side chain is disordered. Both Mg^{2+} atoms are also in their typical positions, octahedrally coordinated to S119, D251, E252, five water molecules, and the PP_i molecule.

The Crystal Structure of *Mtb*-R194A Captures Anthranilate Bound in Three Different Binding Sites. *Mtb*-R194A was crystallized in the presence of PRPP and Mg^{2+} and soaked with anthranilate for 5 min at 4 °C prior to analysis (Table 2, structure E). Electron density indicated that PP_i and Mg^{2+} were present in their typical binding modes,[14] but there was no density present for the ribose ring and phosphate moieties of PRPP, potentially indicating that catalysis had taken place. Each chain has two anthranilate molecules bound within the anthranilate tunnel, occupying sites 1 and 2 in chain A

DOI: 10.1021/acs.biochem.5b00612
Biochemistry 2015, 54, 6082−6092

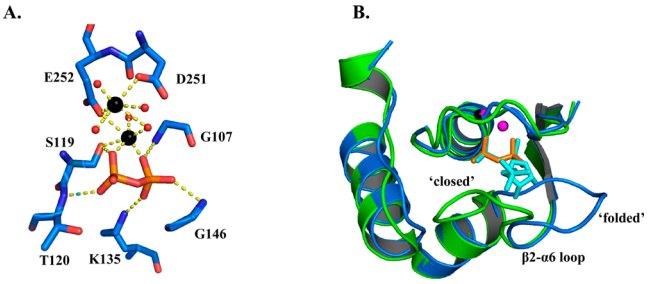

Figure 6. PP_i-Mg binding in *Mtb*-R193L. (A) *Mtb*-R193L (blue) with PP_i (orange) and Mg^{2+} (black spheres) bound postcatalysis. Polar contacts and water molecules are shown as yellow dashes and red spheres, respectively. (B) *Mtb*-R193L (blue) with PP_i and Mg^{2+} bound overlaid on wild-type *Mtb*-AnPRT (green, PDB entry 1ZVW) with PRPP (cyan) and Mg^{2+} (magenta spheres) bound.

(Figure 7A,C) and sites 1 and 3 in chain B (Figure 7B,D). In both chains, the density for the $\beta2-\alpha6$ loop is disordered.

The site 3 anthranilate molecule forms a hydrogen bond to the backbone oxygen of nonconserved residue R187 via a single water molecule and is stacked parallel to the P180 pyrrolidine ring, suggestive of C−H···π interactions,[32,36] and similar to the binding modes of anthranilate-like substrates observed previously.[19] This indicates that the absence of the side chain functionality of R194 is not enough to disrupt site 3 and may provide an explanation for the residual substrate inhibition in this variant (Table 1). The amino moiety of the anthranilate molecule bound in site 2 forms hydrogen bonds with the carboxylate group of the site 1 anthranilate and to invariant residue R193 via a water molecule. The carboxylate group of the site 2 anthranilate forms hydrogen bonds with invariant residue N138 and three water molecules, of which two act as bridging waters to R193 and conserved residue H183. The site 1 anthranilate molecules in either chain make different hydrogen bond contacts, but there is no observable change in protein conformation between chains A and B to account for this difference. The anthranilate tunnel residues (residues within 5 Å of the anthranilate molecules) of chains A and B of structure E can be superimposed with a root-mean-square deviation (rmsd) of 0.37 Å. The site 1 anthranilate adjacent to the site 2 anthranilate forms hydrogen bonds with invariant residues G107 and T108 via its amino group, and with residues R193 and N138, the amino group of the site 2 anthranilate, and three water molecules via its carboxylate group. These three water molecules provide water-mediated hydrogen bonds to N138, G107, N203, and G206, all of which are absolutely conserved. When the secondary anthranilate molecule is in site 3, however, the amino group of the site 1 anthranilate forms hydrogen bonds with both N203 and G206 via a single water molecule, and the carboxylate group forms hydrogen bonds with N138, a nonbridging water, and residues R193 and N138 via two water molecules.

This structure of *Mtb*-R194A (structure E) confirms the ability of the natural substrate anthranilate to occupy each of the three anthranilate sites and is the first example of a *Mtb*-AnPRT variant to capture anthranilate in the catalytically relevant site 1.

DISCUSSION

The ability of an enzyme to make conformational adjustments is critical for its catalytic role and is of paramount importance for informing intelligent drug design, as different enzyme

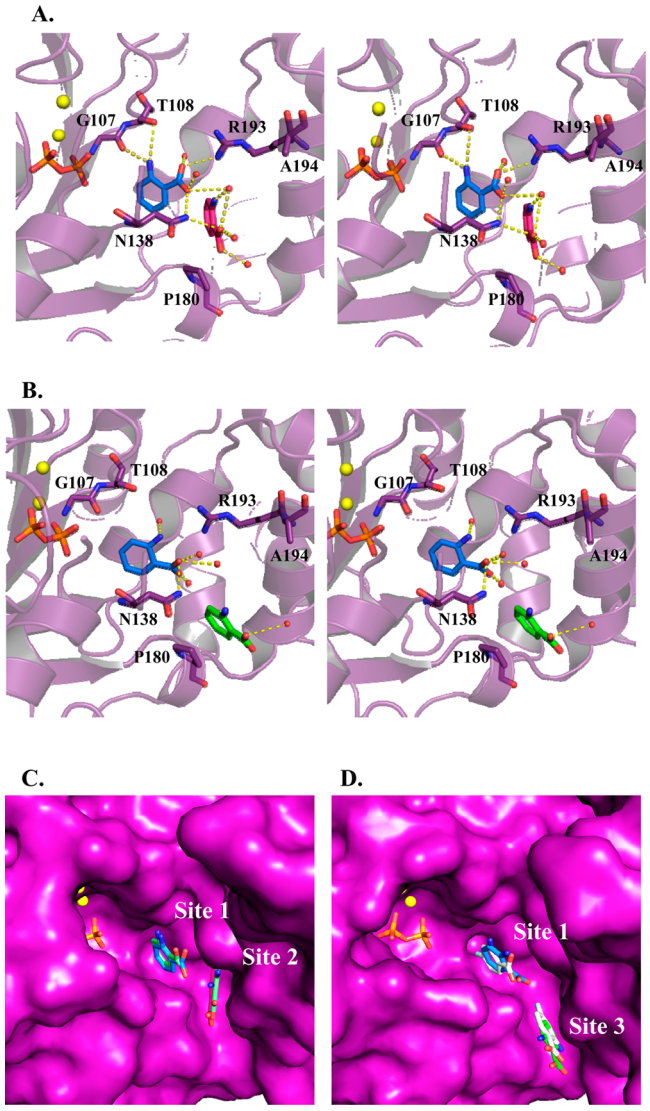

Figure 7. Anthranilate binding sites in *Mtb*-R194A. (A) Stereodiagram of *Mtb*-R194A (structure E) chain A (purple) with PP_i (orange), Mg^{2+} (yellow spheres), and anthranilate bound in both site 1 (blue) and site 2 (pink). (B) Stereodiagram of chain B of structure E with anthranilate bound in both site 1 (blue) and site 3 (green). Hydrogen bonds are shown as yellow dashes with water molecules as red spheres. (C) Surface representation of chain A of structure E with anthranilate bound, overlaid on *Sso*-AnPRT (not shown) with anthranilate (light green) bound (PDB entry 1ZYK). (D) Surface representation of chain B of structure E with anthranilate bound, overlaid on wild-type *Mtb*-AnPRT (not shown) with 4FA (white) bound (PDB entry 4N5V).

conformations may have different binding affinities for particular compounds. The crystal structures of the *Mtb*-AnPRT variants obtained in this study capture the enzyme in differing stages of catalysis and help to illustrate how *Mtb*-AnPRT relies on the movement of the active site $\beta2-\alpha6$ loop between different conformations to facilitate catalysis.

Mtb-AnPRT has the unusual capacity to bind the substrate anthranilate in a number of positions within a tunnel that links the external surface of the protein to the PRPP cosubstrate binding site. Of all the variants created by substituting tunnel residues that were examined, those bearing changes to residue R193 were shown to have the greatest negative impact on catalytic function. Crystal structures of wild-type *Mtb*-AnPRT

DOI: 10.1021/acs.biochem.5b00612
Biochemistry 2015, 54, 6082−6092

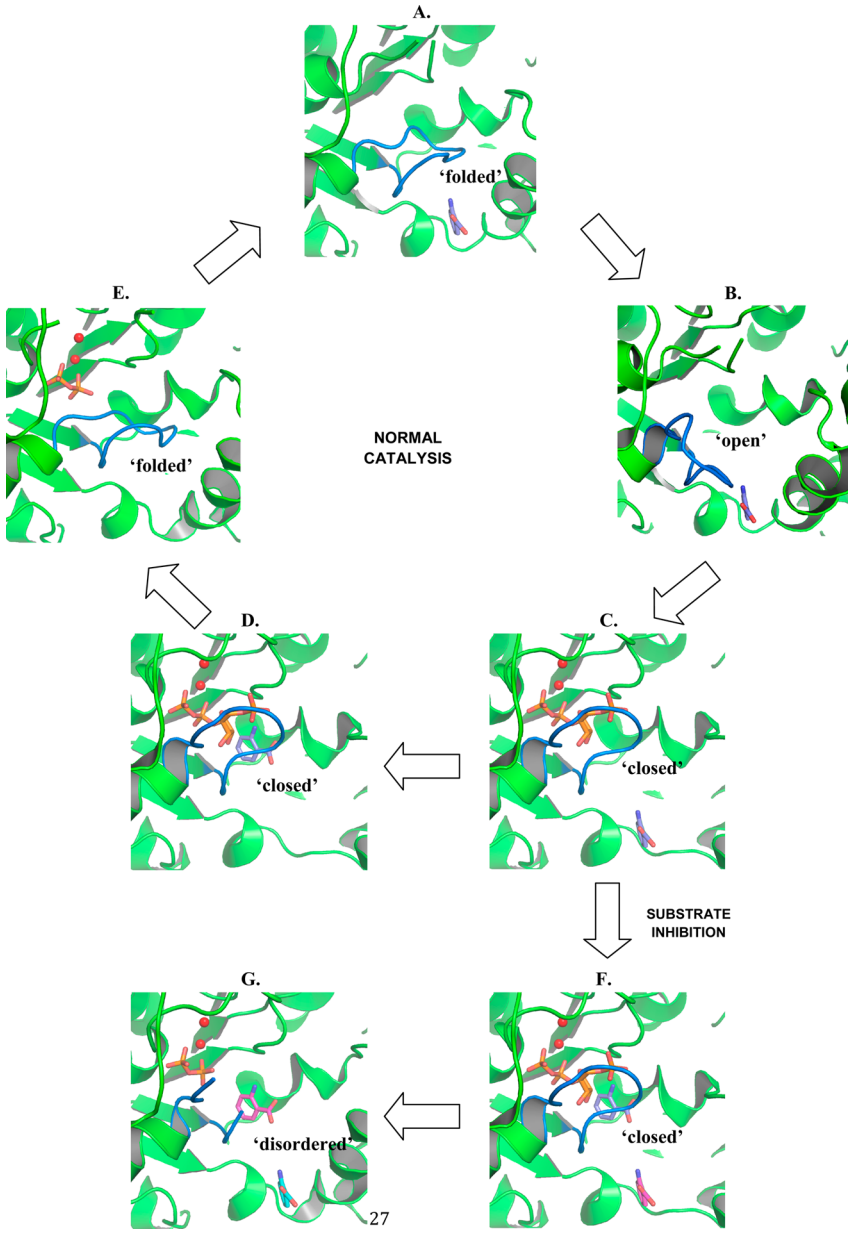

Figure 8. Proposed normal catalytic cycle (A–E) and route for anthranilate substrate inhibition of *Mtb*-AnPRT (F and G). The $\beta2-\alpha6$ loop is colored blue throughout the cycle to highlight its position. (A) Anthranilate 1 (purple, site 3) is shown bound in the active site with the $\beta2-\alpha6$ loop in the "folded" conformation (structure C2). (B) To accommodate PRPP/Mg^{2+} binding, the $\beta2-\alpha6$ loop moves to the "open" position (PDB entry 4OWV). (C) PRPP and Mg^{2+} are bound correctly in the active site with the $\beta2-\alpha6$ loop in the "closed" conformation (structure C2 and PDB entry 1ZVW). (D) The movement of the $\beta2-\alpha6$ loop to the "closed" conformation in panel C leaves the tunnel open for anthranilate 1 to move to the catalytically relevant site 1 (structure E and PDB entry 1ZVW). (E) Catalysis occurs, PRA leaves the active site, and the $\beta2-\alpha6$ loop returns to the "folded" conformation (structure D2). (F) At high anthranilate concentrations, as anthranilate 1 moves to site 1, anthranilate 2 (pink) also binds at site 3 (structure E, structure C2, and PDB entry 1ZVW). (G) After catalysis occurs between PRPP and anthranilate 1, PRA leaves the active site and anthranilate 2 moves to site 1, leaving site 3 available for anthranilate 3 (cyan) to bind. The $\beta2-\alpha6$ loop cannot return to the "folded" conformation, leaving PP_i-Mg potentially trapped within the active site and the enzyme inhibited (structures E and C2).

have demonstrated that R193 forms hydrogen bonds to the carboxylate group of the anthranilate analogue 4FA when it is bound in the inner catalytic site (site 1) (PDB entry 4N5V),[19] and the lower catalytic efficiency of the R193A and R193L variant proteins is consistent with this residue's important role of assisting in anchoring anthranilate in the correct position for efficient reaction with PRPP. Consistent with this role, the structure of *Mtb*-R193A demonstrated anthranilate binding only at site 3. In contrast, the structure of *Mtb*-R194A, a variant with a catalytic efficiency similar to that of wild-type *Mtb*-AnPRT, demonstrates anthranilate binding at sites 1–3.

By comparing all of the variant *Mtb*-AnPRT structures that were captured in the presence of PRPP, Mg^{2+}, and anthranilate, we can begin to propose a possible order of ligand binding events, and the associated conformational adjustments made by this protein to facilitate the catalytic cycle. Figure 8 illustrates a proposed model for the catalytic cycle of *Mtb*-AnPRT, informed by all currently available crystal structures and enzyme kinetics.[14,18–20]

DOI: 10.1021/acs.biochem.5b00612
Biochemistry 2015, 54, 6082–6092

The structure of *Mtb*-R193A with anthranilate bound (structure C2) has demonstrated that anthranilate can bind to the enzyme in nonproductive site 3 without PRPP or Mg^{2+} simultaneously binding. It has previously been suggested that the binding of anthranilate in site 3 precedes PRPP binding.[19] This would allow immediate substitution and reaction once labile PRPP has bound and would increase the efficiency of the *Mtb*-AnPRT reaction. The "folded" conformation of the $\beta2-\alpha6$ loop in structure C2 suggests that the placement of this loop within the anthranilate tunnel is correlated with the binding of anthranilate in site 3 in the absence of PRPP. The wild-type structure obtained from soaking with the anthranilate analogue 4FA for 6 s (PDB entry 4N8Q)[19] also shows the $\beta2-\alpha6$ loop folded into the anthranilate tunnel when 4FA is bound in site 3, indicating that this binding event combined with the "folded" conformation is not unique to the variant structures.[19] The exact role of the "folded" conformation in the catalytic cycle is unclear; it could regulate movement of anthranilate in the anthranilate binding tunnel and/or facilitate the departure of products. The "folded" conformation of the $\beta2-\alpha6$ loop would prevent anthranilate molecules from advancing further into the anthranilate tunnel when PRPP is not bound, as the inner catalytic site 2 is not available. Our proposed model of the normal catalytic cycle of *Mtb*-AnPRT includes the "folded" conformation of the $\beta2-\alpha6$ loop both before and after catalysis has occurred (Figure 8A,E). It also indicates the potential importance of this "folded" conformation in the catalytic cycle, and as a conformation for priming the enzyme for further anthranilate binding at site 3 as PP_i-Mg leaves the active site.

The structures of *Mtb*-N138A, *Mtb*-P180A, and *Mtb*-R193L with PRPP and Mg^{2+} bound (structures A, B, and D1, respectively) all show PRPP and Mg^{2+} bound in conformations identical to those seen in wild-type *Mtb*-AnPRT (PDB entry 1ZVW), with the $\beta2-\alpha6$ loop in the "closed" conformation. Variants *Mtb*-P180A and *Mtb*-R193L also display similar K_M values for binding of PRPP to the wild-type enzyme, indicating a similarity in PRPP binding between wild-type protein and the aforementioned variants, even with the *Mtb*-R193L variant displaying significantly reduced catalytic activity.

The flexible $\beta2-\alpha6$ loop of *Mtb*-AnPRT has previously been shown to occupy an "open" or "closed" conformation in the absence or presence of PRPP, respectively.[14] The two conformations of PRPP observed within structure B suggest that the $\beta2-\alpha6$ loop has the "open" conformation to allow PRPP binding, before moving to the "closed" conformation when PRPP assumes the correct binding position within the active site. The structure of *Mtb*-AnPRT with anthranilate bound (Table S4, PDB entry 4OWV) supports this theory, as anthranilate is bound in site 3 with the $\beta2-\alpha6$ loop in the "open" conformation (Figure 8B).[19] The movement of the $\beta2-\alpha6$ loop from the "open" to "closed" loop conformation could also be associated with the transfer of anthranilate from site 3 to the catalytically relevant site 1.

When structures A, B, C1, and C2 are taken into consideration, it is possible to hypothesize that the *Mtb*-AnPRT catalytic cycle begins with the $\beta2-\alpha6$ loop in the "folded" conformation as anthranilate binds in site 3, with the loop then moving via the "open" conformation that allows PRPP binding to the "closed" conformation once PRPP is correctly bound (Figure 8A–D). The movement of this loop in this way would allow the movement of anthranilate from site 3 to site 1, with the anthranilate tunnel residues all playing their parts in shuttling anthranilate through the tunnel.

The structure of *Mtb*-R193L with PP_i and Mg^{2+} bound (structure D2) shows the $\beta2-\alpha6$ loop folded into the anthranilate tunnel. Assuming that the bound PP_i is a result of reaction between anthranilate and PRPP, representing a complex on the normal reaction pathway and not a dead-end complex, we can infer that the PRA product departs the active site prior to the PP_i-Mg complex. The conformation of the $\beta2-\alpha6$ loop in structure D2 also indicates that movement of this loop from its "closed" conformation (surrounding PRPP or the phosphoribosyl portion of product PRA) to the "folded" conformation within the anthranilate tunnel could potentially be necessary before the PP_i-Mg complex departs the active site. The "folded" conformation leaves the active site more open for PP_i-Mg departure, as shown in Figure 9A–C. Thus, via

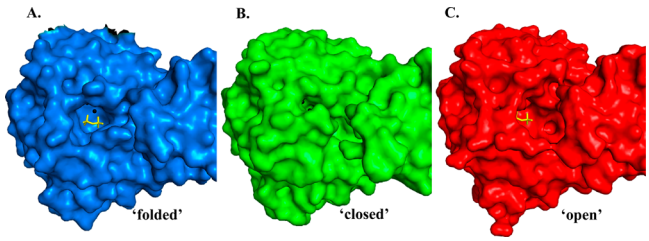

Figure 9. Surface representations of "folded", "closed", and "open" $\beta2-\alpha6$ loop positions. (A) Surface representation of *Mtb*-R193L chain B (blue) with PP_i (yellow) and Mg^{2+} (black spheres) bound (structure D2). (B) Surface representation of wild-type *Mtb*-AnPRT (green, PDB entry 1ZVW) with PRPP (not shown) and Mg^{2+} (not shown) bound. The PP_i and Mg^{2+} from structure D2 are also shown. (C) Surface representation of ligand-free wild-type *Mtb*-AnPRT (red, PDB entry 3QR9). The PP_i and Mg^{2+} from structure D2 are also shown.

comparison of structure D2 to the structure of *Mtb*-R193A with anthranilate bound (structure C2), the conformation of the $\beta2-\alpha6$ loop could be folded into the anthranilate tunnel both before and after catalysis has occurred (Figure 8A,E).

While potentially increasing the efficiency of *Mtb*-AnPRT catalysis, the binding of anthranilate at site 3 has been previously suggested to be responsible also for the substrate inhibition observed at high anthranilate concentrations.[19] Indeed, the substitution of the key residues involved in anthranilate binding in site 3, N138, R194, and P180, with alanine caused a marked increase in the K_i value of anthranilate in *Mtb*-AnPRT, with *Mtb*-N138A showing no capacity for anthranilate inhibition. The structure of *Mtb*-R194A with PP_i, Mg^{2+}, and anthranilate bound (structure E) has likely captured a snapshot of the enzyme in its anthranilate-inhibited state. During catalysis, as the anthranilate molecule in site 1 reacts with the ribose ring of PRPP, it is likely that the $\beta2-\alpha6$ loop is in the "closed" conformation, which can be observed in the wild-type *Mtb*-AnPRT structure with the anthranilate analogue (4FA), PRPP, and Mg^{2+} bound (Table S4, PDB entry 4N5V[19]). This conformation of the $\beta2-\alpha6$ loop would leave the anthranilate tunnel unblocked, and at high anthranilate concentrations, a second anthranilate could occupy site 2 or 3 unimpeded (Figure 8F,G). Following the postreaction evacuation of PRA from the active site, this second anthranilate could migrate further into catalytically relevant site 1.

As the structure of *Mtb*-R193L with PP_i and Mg^{2+} bound (structure D2) suggests, the $\beta2-\alpha6$ loop may be required to fold into the anthranilate tunnel before PP_i-Mg release. The presence of two anthranilate molecules in the anthranilate tunnel of structure E would prevent this loop movement from

DOI: 10.1021/acs.biochem.5b00612
Biochemistry 2015, 54, 6082–6092

occurring, as it is evident that the anthranilate molecules bound in either site 1 or site 2 would block the $\beta2-\alpha6$ loop from taking up the "folded" conformation.

The PP_i-Mg complex observed bound in the active site of structure E may therefore be unable to leave the enzyme for this reason, leaving the active site of *Mtb*-AnPRT effectively blocked. Previous studies have shown that anthranilate-like inhibitors show promising potency, and crystal structures of *Mtb*-AnPRT with these inhibitors bound demonstrate these compounds binding within the anthranilate tunnel, not only preventing anthranilate from binding but also preventing the $\beta2-\alpha6$ loop from folding into the tunnel.[18,20] However, it must be noted that there is as yet no evidence that demonstrates that an anthranilate molecule that binds at the outer site 3 directly becomes a substrate by passage through the anthranilate tunnel within a single *Mtb*-AnPRT molecule.

The flexible $\beta2-\alpha6$ loop could therefore be likened to a traffic signal, with the "folded" conformation akin to a red light with respect to anthranilate movement from site 3 to site 1, and the "closed" conformation a green light, supporting a full and functional active site. Higher concentrations of anthranilate lead to an anthranilate "traffic jam", with the presence of anthranilate in site 1 postreaction rendering the $\beta2-\alpha6$ loop unable to undergo its conformational changes that support catalysis and *Mtb*-AnPRT inhibited. Collectively, these observations and new structures underpin the importance of conformational change in enzyme function.

■ ASSOCIATED CONTENT

Supporting Information

The Supporting Information is available free of charge on the ACS Publications website at DOI: 10.1021/acs.biochem.5b00612.

Collection and refinement data, mass spectral results, circular dichroism spectra of the variants, kinetic plots, and rmsd comparisons (PDF)

■ AUTHOR INFORMATION

Corresponding Author

*E-mail: emily.parker@canterbury.ac.nz.

Present Addresses

§G.L.E.: School of Chemistry and Biochemistry, The University of Western Australia, Crawley 6009, WA, Australia.

∥A.C.: Karolinska Institutet, Department of Microbiology, Tumor and Cell Biology, 171 77 Stockholm, Sweden.

Funding

This work was funded by the Maurice Wilkins Centre for Molecular Biodiscovery. T.V.M.C. was supported by a doctoral scholarship from the Maurice Wilkins Centre for Molecular Biodiscovery.

Notes

The authors declare no competing financial interest.

■ ACKNOWLEDGMENTS

X-ray data were collected at the MX beamlines of the Australian Synchrotron with access through the New Zealand Synchrotron Group.

■ REFERENCES

(1) Upshur, R., Singh, J., and Ford, N. (2009) Apocalypse or redemption: responding to extensively drug-resistant tuberculosis. *Bull. W. H. O. 87*, 481.

(2) Gandhi, N. R., Nunn, P., Dheda, K., Schaaf, H. S., Zignol, M., van Soolingen, D., Jensen, P., and Bayona, J. (2010) Multidrug-resistant and extensively drug-resistant tuberculosis: a threat to global control of tuberculosis. *Lancet 375*, 1830−1843.

(3) Shah, N. S., Wright, A., Bai, G. H., Barrera, L., Boulahbal, F., Martin-Casabona, N., Drobniewski, F., Gilpin, C., Havelkova, M., Lepe, R., Lumb, R., Metchock, B., Portaels, F., Rodrigues, M. F., Rusch-Gerdes, S., Van Deun, A., Vincent, V., Laserson, K., Wells, C., and Cegielski, J. P. (2007) Worldwide emergence of extensively drug-resistant tuberculosis. *Emerging Infect. Dis. 13*, 380−387.

(4) Goldberg, D. E., Siliciano, R. F., and Jacobs, W. R. (2012) Outwitting Evolution: Fighting Drug-Resistant TB, Malaria, and HIV. *Cell 148*, 1271−1283.

(5) Zhang, Y. J., Reddy, M. C., Ioerger, T. R., Rothchild, A. C., Dartois, V., Schuster, B. M., Trauner, A., Wallis, D., Galaviz, S., Huttenhower, C., Sacchettini, J. C., Behar, S. M., and Rubin, E. J. (2013) Tryptophan biosynthesis protects Mycobacteria from CD4 T-cell-mediated killing. *Cell 155*, 1296−1308.

(6) Smith, D. A., Parish, T., Stoker, N. G., and Bancroft, G. J. (2001) Characterization of auxotrophic mutants of *Mycobacterium tuberculosis* and their potential as vaccine candidates. *Infect. Immun. 69*, 1142.

(7) Smith, J. L. (1999) Forming and inhibiting PRT active sites. *Nat. Struct. Biol. 6*, 502−504.

(8) Musick, W. D. L., and Nyhan, W. L. (1981) Structural features of the phosphoribosyl-transferases and their relationship to the human deficiency disorders of purine and pyrimidine metabolism. *Crit. Rev. Biochem. Mol. Biol. 11*, 1−34.

(9) Sinha, S. C., and Smith, J. L. (2001) The PRT protein family. *Curr. Opin. Struct. Biol. 11*, 733−739.

(10) Eads, J. C., Ozturk, D., Wexler, T. B., Grubmeyer, C., and Sacchettini, J. C. (1997) A new function for a common fold: The crystal structure of quinolinic acid phosphoribosyltransferase. *Structure 5*, 47−58.

(11) Chappie, J. S., Cànaves, J. M., Han, G. W., Rife, C. L., Xu, Q., and Stevens, R. C. (2005) The structure of a eukaryotic nicotinic acid phosphoribosyltransferase reveals structural heterogeneity among type II PRTases. *Structure 13*, 1385−1396.

(12) Schramm, V. L., and Grubmeyer, C. (2004) Phosphoribosyl-transferase mechanisms and roles in nucleic acid metabolism. *Prog. Nucleic Acid Res. Mol. Biol. 78*, 261−304.

(13) Ivens, A., Mayans, O., Szadkowski, H., Wilmanns, M., and Kirschner, K. (2001) Purification, characterization and crystallization of thermostable anthranilate phosphoribosyltransferase from Sulfolobus solfataricus. *Eur. J. Biochem. 268*, 2246−2252.

(14) Lee, C. E., Goodfellow, C., Javid-Majd, F., Baker, E. N., and Lott, S. J. (2006) The crystal structure of TrpD, a metabolic enzyme essential for lung colonization by *Mycobacterium tuberculosis*, in complex with its substrate phosphoribosylpyrophosphate. *J. Mol. Biol. 355*, 784−797.

(15) Kim, C., Xuong, N. H., Edwards, S., Madhusudan, Yee, M. C., Spraggon, G., and E Mills, S. (2002) The crystal structure of anthranilate phosphoribosyltransferase from the enterobacterium *Pectobacterium carotovorum*. *FEBS Lett. 523*, 239−246.

(16) Taka, J. (2005) Stabilization due to dimer formation of phosphoribosyl anthranilate isomerase from *Thermus thermophilus* HB8: X-Ray analysis and DSC experiments. *J. Biochem. 137*, 569−578.

(17) Marino, M., Deuss, M., Svergun, D. I., Konarev, P. V., Sterner, R., and Mayans, O. (2006) Structural and mutational analysis of substrate complexation by anthranilate phosphoribosyltransferase from *Sulfolobus solfataricus*. *J. Biol. Chem. 281*, 21410−21421.

(18) Castell, A., Short, F. L., Evans, G. L., Cookson, T. V. M, Bulloch, E. M. M., Joseph, D. D. A., Lee, C. E., Parker, E. J., Baker, E. N., and Lott, J. S. (2013) Substrate capture mechanism of *Mycobacterium tuberculosis* anthranilate phosphoribosyltransferase provides a mode for inhibition. *Biochemistry 52*, 1776−1787.

DOI: 10.1021/acs.biochem.5b00612
Biochemistry 2015, 54, 6082−6092

(19) Cookson, T. V. M, Castell, A., Bulloch, E., Short, F., Evans, G. L., Baker, E. N., Lott, J. S., and Parker, E. J. (2014) Alternative substrates reveal catalytic cycle and key binding events in the reaction catalysed by anthranilate phosphoribosyltransferase from *Mycobacterium tuberculosis*. *Biochem. J. 461*, 87−98.
(20) Evans, G. L., Gamage, S. A., Bulloch, E. M. M., Baker, E. N., Denny, W. A., and Lott, J. S. (2014) Repurposing the chemical scaffold of the anti-arthritic drug lobenzarit to target tryptophan biosynthesis in *Mycobacterium tuberculosis*. *ChemBioChem 15*, 852−864.
(21) de Marco, A. (2011) Molecular and chemical chaperones for improving the yields of soluble recombinant proteins. *Methods Mol. Biol. (N. Y., NY, U. S.) 705*, 31−51.
(22) Kabsch, W. (2010) XDS. *Acta Crystallogr., Sect. D: Biol. Crystallogr. 66*, 125−132.
(23) Evans, P. (2006) Scaling and assessment of data quality. *Acta Crystallogr., Sect. D: Biol. Crystallogr. 62*, 72−82.
(24) Winn, M. D., Ballard, C. C., Cowtan, K. D., Dodson, E. J., Emsley, P., Evans, P. R., Keegan, R. M., Krissinel, E. B., Leslie, A. G. W., McCoy, A., McNicholas, S. J., Murshudov, G. N., Pannu, N. S., Potterton, E. A., Powell, H. R., Read, R. J., Vagin, A., and Wilson, K. S. (2011) Overview of the CCP4 suite and current developments. *Acta Crystallogr., Sect. D: Biol. Crystallogr. 67*, 235−242.
(25) McCoy, A. J., Grosse-Kunstleve, R. W., Adams, P. D., Winn, M. D., Storoni, L. C., and Read, R. J. (2007) Phaser crystallographic software. *J. Appl. Crystallogr. 40*, 658−674.
(26) Murshudov, G. N., Skubak, P., Lebedev, A. A., Pannu, N. S., Steiner, R. A., Nicholls, R. A., Winn, M. D., Long, F., and Vagin, A. A. (2011) REFMAC5 for the refinement of macromolecular crystal structures. *Acta Crystallogr., Sect. D: Biol. Crystallogr. 67*, 355−367.
(27) Emsley, P., and Cowtan, K. (2004) Coot: model-building tools for molecular graphics. *Acta Crystallogr., Sect. D: Biol. Crystallogr. 60*, 2126−2132.
(28) Chen, V. B., Arendall, W. B., III, Headd, J. J., Keedy, D. A., Immormino, R. M., Kapral, G. J., Murray, L. W., Richardson, J. S., and Richardson, D. C. (2010) MolProbity: all-atom structure validation for macromolecular crystallography. *Acta Crystallogr., Sect. D: Biol. Crystallogr. 66*, 12−21.
(29) Schuttelkopf, A. W., and van Aalten, D. M. F. (2004) PRODRG: a tool for high-throughput crystallography of protein-ligand complexes. *Acta Crystallogr., Sect. D: Biol. Crystallogr. 60*, 1355−1363.
(30) *The PyMOL Molecular Graphics System*, version 1.5.0 (2012) Schrodinger, LLC, Portland, OR.
(31) Read, R. J., and Schierbeek, A. J. (1988) A phased translation function. *J. Appl. Crystallogr. 21*, 490−495.
(32) Brandl, M., Weiss, M. S., Jabs, A., Suhnel, J., and Hilgenfeld, R. (2001) C-H···pi-interactions in proteins. *J. Mol. Biol. 307*, 357−377.
(33) Armougom, F., Moretti, S., Poirot, O., Audic, S., Dumas, P., Schaeli, B., Keduas, V., and Notredame, C. (2006) Expresso: automatic incorporation of structural information in multiple sequence alignments using 3D-coffee. *Nucleic Acids Res. 34*, W604−W608.
(34) Gouet, P., Courcelle, E., Stuart, D. I., and Métoz, F. (1999) ESPript: analysis of multiple sequence alignments in PostScript. *Bioinformatics 15*, 305−308.
(35) Schlee, S., Deuss, M., Bruning, M., Ivens, A., Schwab, T., Hellmann, N., Mayans, O., and Sterner, R. (2009) Activation of anthranilate phosphoribosyltransferase from *Sulfolobus solfataricus* by removal of magnesium inhibition and acceleration of product release. *Biochemistry 48*, 5199−5209.
(36) Scheiner, S., Kar, T., and Pattanayak, J. (2002) Comparison of various types of hydrogen bonds involving aromatic amino acids. *J. Am. Chem. Soc. 124*, 13257−13264.

DOI: 10.1021/acs.biochem.5b00612
Biochemistry 2015, 54, 6082−6092